Bulk electro-optic deflector-based switches

Yiying Zuo,[1,*] Madeleine Mony,[1] Babak Bahamin,[1] Etienne Grondin,[2] Vincent Aimez,[2] and David V. Plant[1]

[1]Department of Electrical and Computer Engineering, McGill University, Montréal, Québec H3A 2A7, Canada
[2]Department of Electrical and Computer Engineering, Université de Sherbrooke, Sherbrooke, Québec J1K 2R1, Canada

*Corresponding author: yiyingzuo@yahoo.com

Received 18 December 2006; revised 16 February 2007; accepted 16 February 2007;
posted 21 February 2007 (Doc. ID 78219); published 15 May 2007

We propose two novel electro-optic (EO) deflectors based on two new nonrectangular geometries: the parabolic and the half-horn configurations. These devices not only provide excellent deflection angles, but also have the potential to build nonblocking 2×2 optical switches. A deflector figure of merit is defined, and comparisons with existing EO deflectors are given. Devices fabricated in $LiTaO_3$ demonstrate 3 dB of average insertion loss and 3° deflection angles. These results represent the best deflection performances to our knowledge reported to date for bulk EO deflectors. © 2007 Optical Society of America

OCIS codes: 230.0230, 230.2090.

1. Introduction

Electro-optic (EO) beam deflectors are extensively used in optical switches, beam scanners, optical displays, printing, and space tracking and acquisition, as well as laser control [1]. These devices exhibit high bandwidth, fast response time, moderate deflection, and low power consumption and are generally compact when compared with other deflectors. Given these benefits, EO switches with high speed and low loss have been built for future agile optical networks [2–4].

To fabricate EO deflectors, ferroelectric crystals such as $LiTaO_3$ or $LiNbO_3$ are first poled to provide the required predefined domain structures [5,6]. The application of an electrical field across the crystal then produces different indices in the two domains, and the light beam is deflected through refraction as it passes through the poled wafer.

Domains with rectangular contours were implemented in EO deflectors and EO scanners [7,8]. Other domain configurations, such as trapezoidal and horn contours, were also reported as beam scanners [9–11].

We propose two novel EO deflectors with excellent beam bending performances. The new geometries for the domain configurations are first derived by using an equivalency theory we developed for nonrectangular configurations of prisms in EO deflectors. Based on these new geometries, EO deflectors are designed, simulated, fabricated, and tested. The concept of a nonblocking 2×2 optical switch based on these EO deflectors is also presented.

In Section 2 we describe the basic processes of light beam steering by refraction. The devices with rectangular contours are analyzed, and the upper bound of the bending angle is quantified for the first time. Then, an equivalence theory for a gradient-index structure is introduced as a convenient alternative for the design and analysis of EO deflectors with nonrectangular contours. In Section 3 we propose new designs for EO deflectors. New geometries, such as parabolic and half-horn configurations, are derived for the first time, to the best of our knowledge. They exhibit the best-known steering performance among all bulk EO deflectors reported to date. Employing these new geometries, novel EO deflectors are designed, and the concept of nonblocking 2×2 optical switches is presented. A deflector figure of merit is proposed in Section 3 to compare different configurations of EO deflectors. Finally, simulations and experimental results of devices are demonstrated in Sections 4 and 5, respectively.

2. Theory

A. Refraction-Based Electro-Optic Deflectors

EO beam deflectors are voltage-controlled, refraction-based devices. Domains of concatenated prisms in EO

0003-6935/07/163323-09$15.00/0

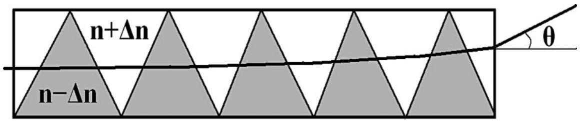

Fig. 1. Domains with concatenated prisms.

crystals (the dark regions within Fig. 1) are inverted by electric field poling [2,12]. An external uniform electrical field applied across the crystal can induce an index change of opposite magnitude on the adjacent domain regions, causing the optical beam to refract at the interfaces. By defining the contour of the prism sequence, the travel path of the light beam can be determined.

According to the EO effect, the refractive index of EO crystals is modified when voltages are applied to the crystals:

$$\Delta n = \frac{1}{2} n^3 r_{33} \frac{V}{D}. \tag{1}$$

Here, n is the original index, r_{33} is the corresponding EO coefficient of the substrate along the z axis, V is the applied electric field along the direction of the dielectric polarization, and D is the thickness of the substrate.

In each prism, the light beam bends up when it travels from a higher-index region ($n + \Delta n$) to a lower-index region ($n - \Delta n$). Given that Δn is of the order of 10^{-3}, as well as the fact that the incident and output angles are typically small, the deflection angle of one prism is governed by

$$\Delta\theta = \frac{4\Delta n}{n} \tan\left(\frac{\beta}{2}\right). \tag{2}$$

For the entire prism sequence, the total deflection angle is expressed by

$$\theta = \sum_i \frac{4\Delta n}{n} \tan\left(\frac{\beta}{2}\right) = \frac{4\Delta n}{n} \sum_i \frac{L_i/2}{W_i}, \tag{3}$$

where L_i is the length of each prism and W_i is the width of each prism. The relationship given by Eq. (3) forms the basis of the analysis of the performance of EO deflectors with rectangular contours as presented in the next subsection.

B. Rectangular Devices and Their Limitations

A well-studied domain configuration is a rectangular contour [8] with a deflection angle of

$$\theta = \frac{4\Delta n}{n} \sum_i \frac{L_i/2}{W_i} = \frac{2\Delta n}{n} \frac{L}{W}, \tag{4}$$

where L is the total length and W is the uniform width of the device.

Though they have a simple configuration, rectangular devices have a limit on the maximum deflection angle they can provide. The device width must be much larger than the spot size of the incident beam to accommodate the full bipolar deflection of the beam at the exit. Thus, the width is unnecessarily large, and deflection angle θ is thus restrained. The limitation of the rectangular deflector is quantified for the first time as follows.

The relationships among length L, width W, beam waist w_a, and deflection angle θ have to follow the following two relationships:

$$W^2 = w_a W + \frac{L^2 n^2 r_{33} V}{D}, \tag{5a}$$

$$W = w_a + \theta L. \tag{5b}$$

Since $W > w_a$, we get

$$\theta < \left(n^2 r_{33} V/D\right)^{1/2}. \tag{6}$$

Assuming that a minimum of 11 prisms is required [9] inside each device and that all prisms have an identical apex angle of 60°, we get the following:

$$L/W > 11 \times 2 \times \tan(30°) \approx 13, \tag{7a}$$

$$\theta > 13 n^2 r_{33} V/D. \tag{7b}$$

Equations (7b) and (6) lead us to

$$13 n^2 r_{33} V/D < \theta < \left(n^2 r_{33} V/D\right)^{1/2}. \tag{8}$$

Therefore, the deflection angle of rectangular devices has an upper bound. In bulk material with V/D of 1/500 kV/μm, r_{33} of 30×10^{-12} m/V, θ has a maximum value of 17 mrad. Even when V/D is 1/150 kV/μm, θ is still limited to 31 mrad. These results demonstrate that, regardless of the device dimension, the deflection angle obtained using rectangular devices is always smaller than $(n^2 r_{33} V/D)^{1/2}$.

C. Equivalency Theory

Equation (3) reveals that the deflection angle can be calculated by summing all the angles in each prism and that calculation is complicated in the nonrectangular devices. To simplify the problem, another device structure with a gradient index within the same contour serves as an alternative in the analysis.

Previous literature [9] has proved that, in rectangular devices, a device structure with a graded-index profile demonstrates the same deflection behaviors as an iterated-prism device. Here, we extend that equivalency theorem to nonrectangular configurations.

Two structures are built with the same contours as shown in Fig. 2. Figure 2(a) has the iterated-prism structure with different indices in two domains, and the vertices of the prisms define the contour of the

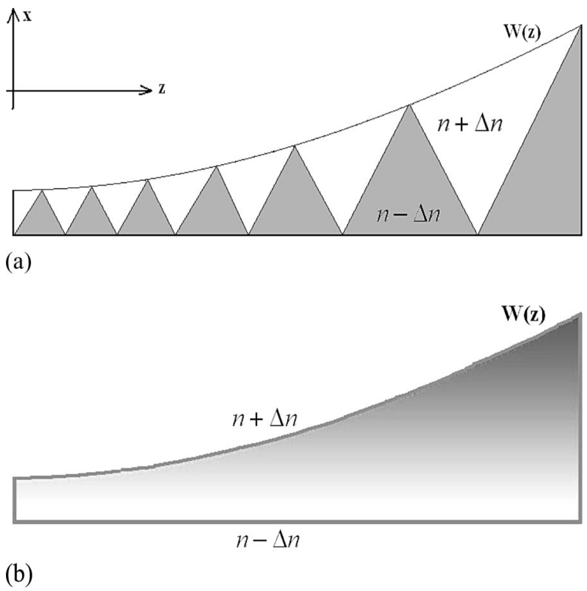

Fig. 2. Two types of deflector structure: (a) iterated prism and (b) gradient index.

deflector. Figure 2(b) has the same contour as Fig. 2(a), with a gradient index along the width. The index within the structure linearly changes from $n - \Delta n$ on the bottom of the contour to $n + \Delta n$ on the top edge of the device as expressed in Eq. (9):

$$\frac{\partial n}{\partial x} = \frac{2\Delta n}{W(z)}, \tag{9}$$

where $W(z)$ is the device width at different z locations. A light ray inside a gradient-index material will obey Eq. (10) [13], where n is a function of variables of x and z as described in Eq. (9):

$$\frac{\mathrm{d}^2 x}{\mathrm{d}z^2} = \frac{\mathrm{d}\theta}{\mathrm{d}z} = \frac{\nabla n}{n} = \frac{1}{n}\frac{\partial n}{\partial x}. \tag{10}$$

The function of the upper contour lines, as well as the deflection angle, is given by Eqs. (11) and (12):

$$\frac{\mathrm{d}^2 x}{\mathrm{d}z^2} = \frac{2\Delta n}{n}\frac{1}{W(z)}, \tag{11}$$

$$\Delta\theta = \int \frac{2\Delta n}{n}\frac{1}{W(z)}\,\mathrm{d}z. \tag{12}$$

The integration in the z direction of the gradient-index structure we defined can be expressed as a summation of the contribution of small regions, with each one corresponding to one prism. Equation (12) can then be simplified to

$$\theta = \int \frac{2\Delta n}{n}\frac{1}{W(z)}\,\mathrm{d}z = \sum_i \frac{2\Delta n}{n}\frac{z_i}{W_i} = \frac{4\Delta n}{n}\sum_i \frac{L_i/2}{W_i}. \tag{13}$$

Comparing Eqs. (3) and (13), we conclude that the deflection behaviors of the iterated-prism structure and the gradient-index structure are identical for any EO device configuration. Given this equivalency in the design and analysis of nonrectangular contoured prism domain structures, simple equations can be employed to determine the performance of such EO deflectors. Without such an equivalency, complicated trigonometric function derivations and calculations would need to be employed, needlessly increasing the complexity of studying such EO devices. In the next sections, optimal designs are derived from the gradient-index structure, and the simulations of the new shaped deflectors in this paper are also based on the gradient-index structure.

3. Novel Designs for Electro-Optic Deflector-Based Switches

A. Optimal Geometry Design for Switches

Previous literature has derived optimal designs for optical scanners [9]. For optical EO scanners, continuous analog voltages are used to deflect the beam over a range of angles. In this section optimal designs are proposed for optical switches as opposed to optical scanners. That is to say, instead of applying continuous analog voltages to the devices, only discrete values of voltage are applied, providing discrete output beam trajectories or output ports. Thus the optimal configurations needed to achieve the best performances for EO switches are different from those for EO scanners.

Ideally, the best deflection performance can be reached if the shape of the deflector perfectly matches the beam trajectory. Specifically, the design with the best deflection performance should satisfy the following two requirements. First, the entire light beam needs to be encapsulated by the prism structures to reduce the exhibited insertion loss. Second, the center of the light beam should meet the interfaces of each prism at its center as shown in Fig. 3. These

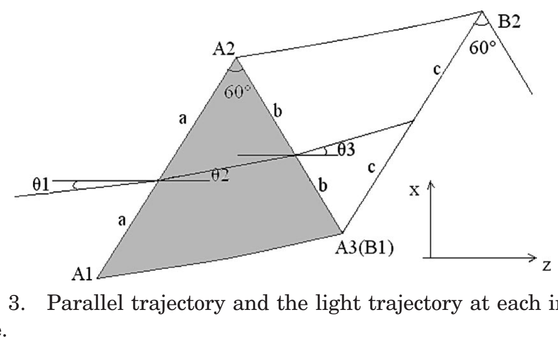

Fig. 3. Parallel trajectory and the light trajectory at each interface.

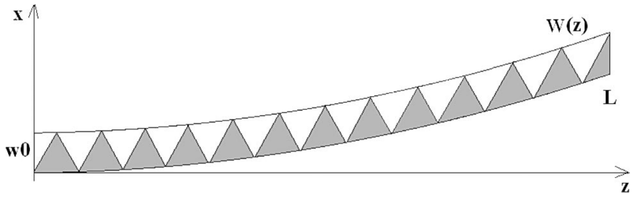

Fig. 4. Parabola device using a prism sequence.

conditions ensure the achievement of the largest beam spot as well as the minimum transmission loss.

Assume that all prisms have an identical apex angle of 60°, which guarantee a less than 0.1% reflection loss in the interfaces. As shown in Fig. 3, a two-prism model with a lower index in the dark region has been demonstrated for analysis. The two prisms have the same vertex angles, $\beta = 60°$. The light beam meets the interfaces of the prisms at the center of A1A2, A2A3, and A3B2. Assuming that the incidence angle and refractive angle at each interface are θ_1, θ_2, and θ_2, θ_3, the length c is derived and calculated as follows:

$$\begin{aligned} c &= b\,\frac{\sin(\beta+\theta_3)}{\sin(\beta-\theta_3)} = a\,\frac{\sin(\beta+\theta_3)}{\sin(\beta-\theta_3)}\,\frac{\sin(\beta-\theta_2)}{\sin(\beta+\theta_2)} \\ &= a\,\frac{\cos(2\beta+\theta_3-\theta_2)-\cos(\theta_2+\theta_3)}{\cos(2\beta+\theta_3-\theta_2)-\cos(\theta_2+\theta_3)}. \end{aligned} \tag{14}$$

Since $\theta_3 - \theta_2$ is typically very small, $c \approx a$, which means that all the prisms are identical. Thus, the top and bottom edges of the device are parallel, and the prism width W_0 is constant.

Assuming a zero initial incidence angle, the total deflection angle and the top edge of the device $W(z)$ can be derived according to Eqs. (11) and (12) as

$$\theta = \frac{4\Delta n}{n}\sum_i \frac{L_i/2}{W_i} = \frac{2\Delta n}{nW_0}\,L, \tag{15}$$

$$W(z) = \frac{\Delta n}{nW_0}\,z^2, \tag{16}$$

where z is the z-axis value of the device end.

Equation (16) indicates that the configuration of the EO deflector, as well as the light beam, follows a parabolic trajectory as illustrated in Fig. 4.

B. Optimal Geometry Design for Switches with a Nonuniform Width

Employing the equivalent theory, EO devices with various configurations can easily be proposed, such as trapezoidal and horn scanners [5,6]. We modified those designs to improve their deflection performances and obtained a half-horn deflector switch as shown in Fig. 5. In the half-horn configuration, the alternative gradient-index structure with the same contour is utilized, and the index change along the x direction at different z is defined as

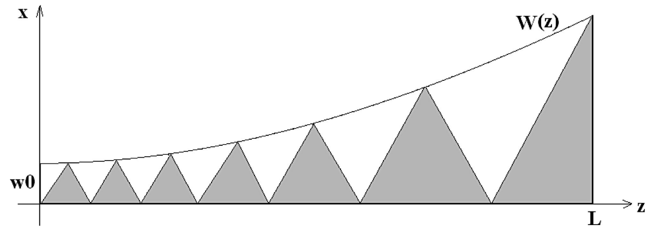

Fig. 5. Half-horn device using a prism sequence.

$$n(x, z) = n - \Delta n + \frac{2\Delta n}{W(z)}\,x, \tag{17}$$

where x is the x-axis value of any point. According to Eq. (10), the top edge follows

$$\frac{\mathrm{d}W}{\mathrm{d}z} = \left[\frac{4\Delta n}{n}\ln\left(\frac{W(z)}{W_0}\right)\right]^{1/2}, \tag{18}$$

where $W(z)$ is the width of the device along the z axis and W_0 is the width at the input end. At the output end of the device ($z = L$),

$$\theta = \left[\frac{4\Delta n}{n}\ln\left(\frac{W(L)}{W_0}\right)\right]^{1/2}. \tag{19}$$

Numerical solutions are readily obtained, since no closed-form solution of $W(z)$ can be derived from Eq. (18).

C. New Deflectors

Based on the new geometries in Subsections 3.A and 3.B, two novel optimally designed EO devices, the half-horn and the parabola deflectors, are proposed as shown in Fig. 6. In both structures, when a constant voltage is applied, the trajectory of the light beam incident from Input A is diverted as it travels through the prism sequence regions. Refractive beam

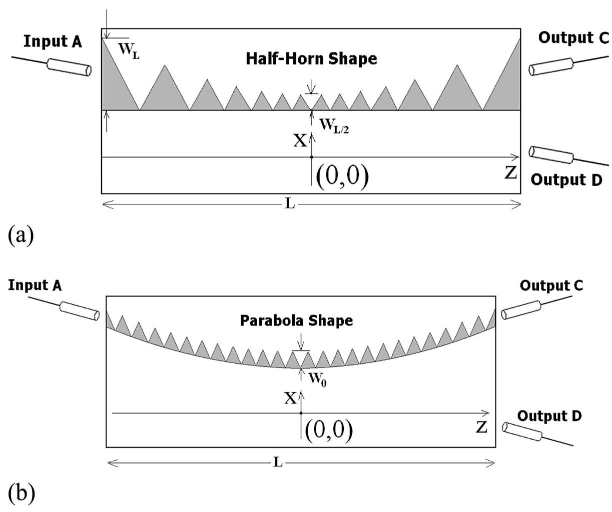

Fig. 6. Schematics of two different deflectors: (a) half-horn and (b) parabola.

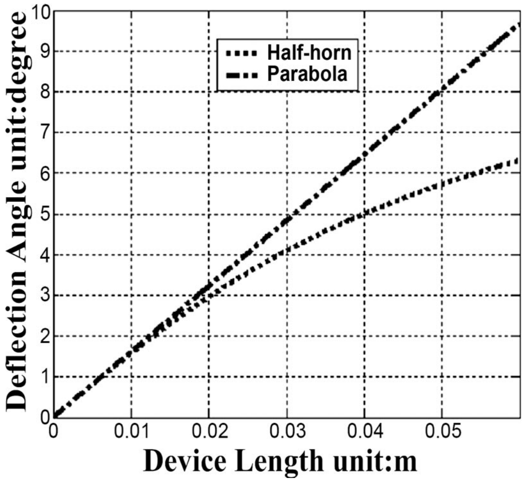

Fig. 7. Deflection angles of the half-horn and parabola deflectors when the device length changes.

deflection occurs at the boundaries of the prisms, and the outgoing beam is detected by the receiving collimator C. When no voltage is applied, the incoming light beam from collimator A travels along a straight line and is collected by collimator D.

Following the same derivation strategy as shown in Eqs. (14)–(18), the deflection angles of the half-horn and parabola devices are given as follows:

$$\theta_{\text{half-horn}} = 2\left[\frac{4\Delta n}{n}\ln\left(\frac{W_L}{W_{L/2}}\right)\right]^{1/2}, \quad (20)$$

$$\theta_{\text{parabola}} = 2\Delta n L/(nW_0). \quad (21)$$

Here L is the length of the device, W_0 is the height of each prism in the parabola device, and $W_L/W_{L/2}$ is the height of the largest/smallest prism in the half-horn device.

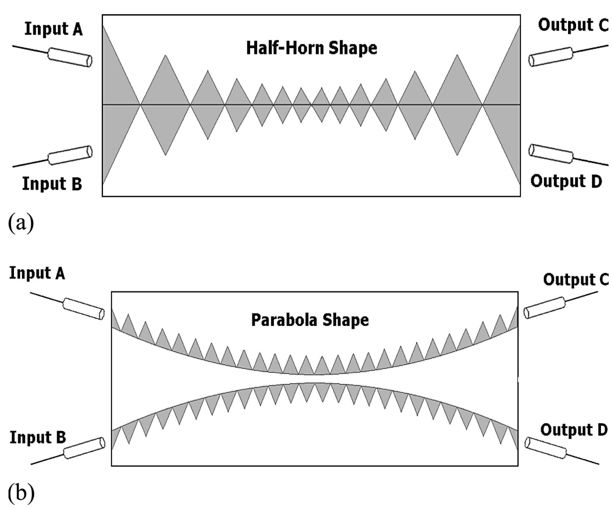

Fig. 8. Schematic of 2 × 2 switches using (a) half-horn geometries and (b) parabola geometries.

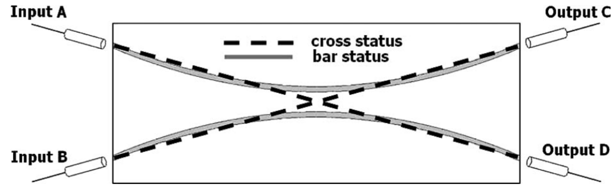

Fig. 9. Cross and bar status of the nonblocking optical switch based on the EO deflectors, with distance between two channels.

Assume that a bulk device that is built in $LiTaO_3$ (index 2.18) has an index change Δn of 10^{-3}. Assume that the width of the two devices $W_{L/2}$ and W_0 is 450 μm. When the device length L increases, the deflection angles in these two devices increase as Fig. 7 shows. As shown in the plot, the increase in deflection angle as the device length increases is greater for the parabola device than for the half-horn device.

Nonblocking 2 × 2 optical switches can be constructed based on these deflectors by vertically mirroring the structure and introducing a second incident collimator B into the deflectors as shown in Fig. 8. The light beam from B travels along a straight line and is detected by collimator C when there is no external voltage. If a stable voltage is applied, the light beam incoming from B will travel alongside the predefined half-horn (or parabolic) trajectory and will be collected by collimator D at the output. The bar and cross status of the switches can be obtained, as shown in Fig. 9.

The distance between the upper and the lower deflectors that make up the 2 × 2 switch must be carefully controlled as shown in Fig. 9. If the distance between the two structures is not correct, the two output locations for the upper deflector will not overlap with the two output locations of the lower deflector, leading to higher insertion losses for the switch. The following expressions provide the ideal distance between the upper and the lower deflectors for both the parabola and the half-horn devices:

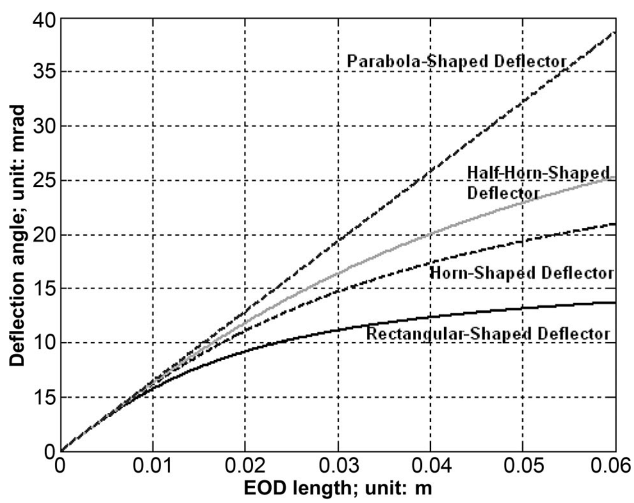

Fig. 10. Deflection angles for different devices.

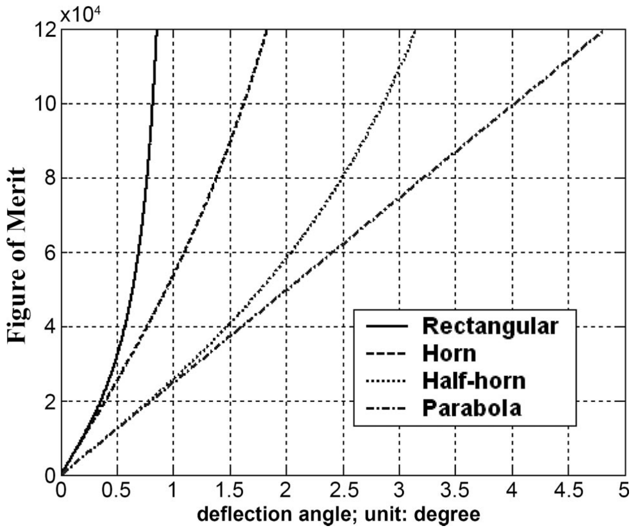

Fig. 11. Deflector figure of merit for different devices.

$$\mathrm{dis}_{\mathrm{parabola}} = \frac{2\Delta n}{nW} L^2 - W, \tag{22}$$

$$\mathrm{dis}_{\text{half-horn}} = 2\left\{L\left[\frac{4\Delta n}{n}\ln\left(\frac{W_L}{W_{L/2}}\right)\right]^{1/2} - W_L\right\} + W_{L/2}. \tag{23}$$

Equations (22) and (23) indicate that once the width and the length of the device are determined, the distance between two channels can be calculated. Also, the deflection angle and the device length increase when the distance between the two channels increases, which benefits the switch design.

D. Deflector Figure of Merit

In the literature, deflection sensitivity is typically defined as the deflection angle per applied volt [7]. However, Eqs. (3) and (12) reveal that the total beam steering angle is dependent on several variables such as the length, the initial width, the configuration of the device, the thickness of the substrate, and the applied electric field. In an attempt to compare all devices, we suggest that the product of the applied electric field and the electrode length be used to de-

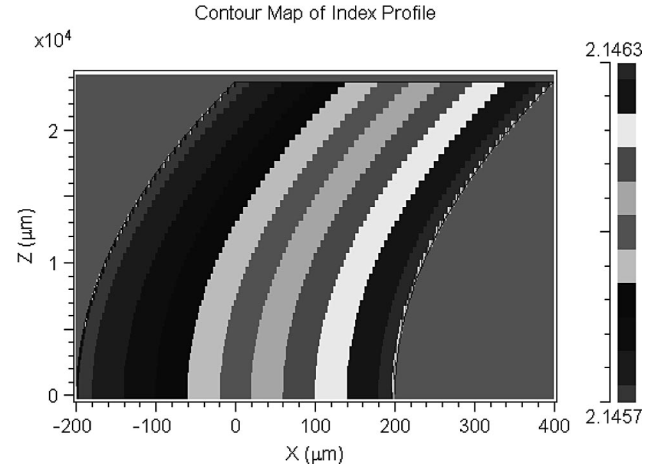

Fig. 12. Index profile of the parabola devices.

fine a figure of merit for the EO deflectors. Although it is the first time this product has been applied to EO deflectors, it is frequently used for EO modulators [14]. With this definition, the product that we define as a deflector figure of merit is given by

$$\text{deflector figure of merit} = VL/D, \tag{24}$$

where V is the applied voltage on the device, D is the thickness of the substrate, and L is the device length. The term V/D is the electrical field in the device. According to this definition, it is clear that better performance is achievable at lower V and shorter L, and thus the deflector figure of merit is better when its value is smaller.

For a given device length and applied electric field, a comparison of Eqs. (4), (15), and (19) indicates that the parabolic device will provide a deflection far greater than that obtained by using a traditional rectangular device. Figure 10 shows the deflection angles obtained by using the rectangular, horn, half-horn, and parabolic configurations. Here, a 1310 nm wavelength, a device entrance width of 450 μm, an applied voltage of 1000 V, and a 500 μm thick z-cut $LiTaO_3$ crystal were assumed. It is shown that even if the device length increases, the deflection angle of the rectangular device cannot exceed 15 mrad. The fig-

Table 1. Comparison of Designs

Type	Length (mm) × Width (μm)	Deflection Angle (mrad)	Figure of Merit (×10^4)
Bulk			
Parabola	40 × 450	25.8	31
Half-horn	40 × 450	20	40
Rectangular [7]	10 × 750	2.3	52
Horn	40 × 450	11	73
Thin substrate			
Parabola	10 × 92	105	6.4
Rectangular [8]	10 × 100	12	8.3
Half-horn	10 × 92	55	12
Horn [11]	10 × 92(678)	41.7	16

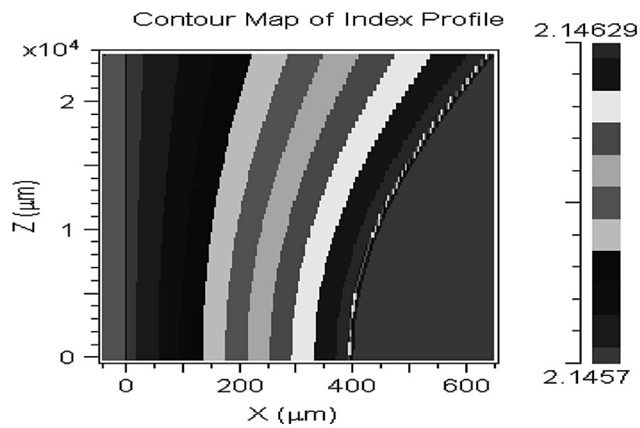

Fig. 13. Index profile of the half-horn devices.

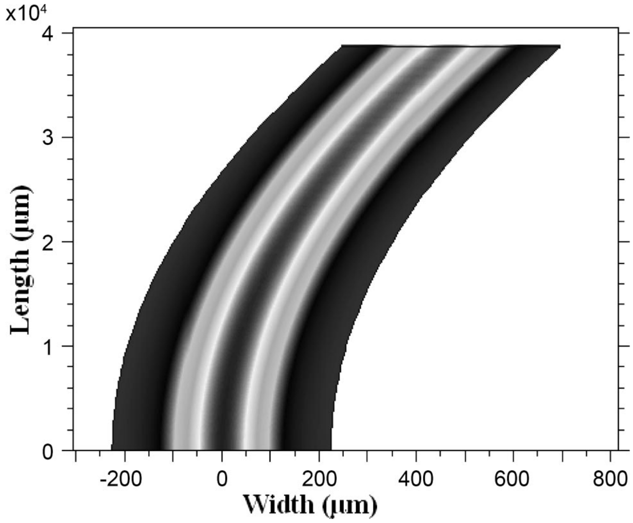

Fig. 14. Beam transmission within the parabola deflectors in BPM simulation.

ures of merit for different deflection angles of these devices are calculated and plotted in Fig. 11. To obtain 1° of deflection angle, Fig. 11 shows that figures of merit of 15×10^4, 5.4×10^4, 2.6×10^4, and 2.5×10^4 are required in the rectangular, horn, half-horn, and parabolic geometries, respectively. Also, since the figure of merit is a nonlinear function of the deflection angle, larger values are needed for the first three configurations when a larger deflection angle is required, as indicated in Fig. 11. These results indicate that under similar dimension conditions, the parabola device has the best deflection performance.

Table 1 summarizes the values (simulated and experimental) of figures of merit for different devices obtained by using Eq. (24). The results show that the parabola and the rectangular devices usually have the smallest value (and therefore the best performance); the half-horn device has the second smallest

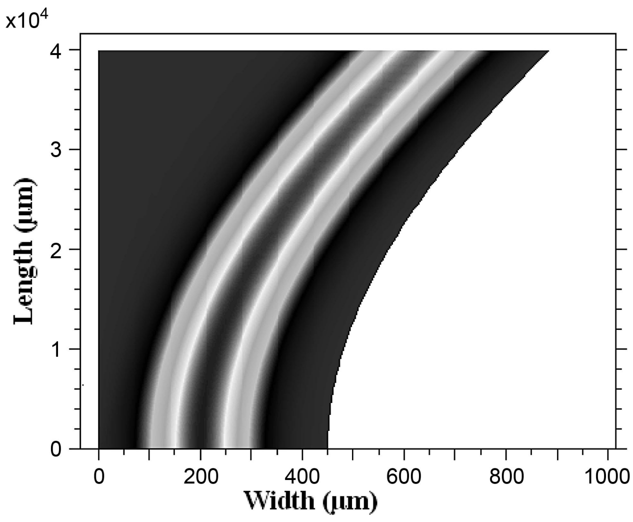

Fig. 15. Beam transmission within the half-horn deflectors in BPM simulation.

Table 2. Simulation Comparisons

Shape	Length (mm) × Width (μm)	Meas./Theor. Deflection Angle (°)
Parabola	41.8 × 500	2.24/3.01
	38.6 × 450	2.74/3.09
Half-horn	40.1 × 450	2.45/2.45
	39.3 × 500	2.2/2.3
Horn	39.6 × 500	1.17/1.3
Rectangular	40 × 612	NA/1.18

value, followed by the horn and the trapezoidal devices. The limitation of the rectangular devices has been introduced in previous sections. For clarity, the table also distinguishes between bulk and thin-film devices. Deflectors can be built with either bulk materials (500 μm thick) or thin wafers (100–150 μm thick), and the profiles of the incident light beam are different for these two types. Also, the typical applied voltage in bulk-based EO deflectors is approximately 1000 V; this voltage is lower in thin-substrate devices.

4. Simulations and Experiments

A. Simulations of New Configurations

Simulations are performed to verify the design of the new deflector configurations. Device models with gradient-index structures as in Figs. 4 and 5 are built with R-Soft BPM (beam propagation method). We assume that the $LiTaO_3$ substrate has a refractive index change of 6×10^{-4} for every 1000 V of applied voltage with a 1310 nm incident beam, and we assume that the device length is 40 mm, that the entrance widths of two new contours are set to 450 μm, and that the exit width of the half-horn is set to 895 μm. The profiles of the gradient index in the BPM are shown in Figs. 12 and 13. The beam transmissions within these devices are shown in Figs. 14 and 15. Table 2 summarizes the design parameters and the theoretical and BPM results. The simulated output deflection angles are 3.0° and 2.4° for the parabola and half-horn deflectors, respectively, and they fit well with the theoretical values. Compared with the deflection performance of the original horn (1.3°) and rectangular (1.18°) deflectors, these two new designs provide a steering improvement factor of approximately 2 to 3.

These configurations are fabricated in 500 μm thick z-cut $LiTaO_3$ wafers. Figure 16 shows the two

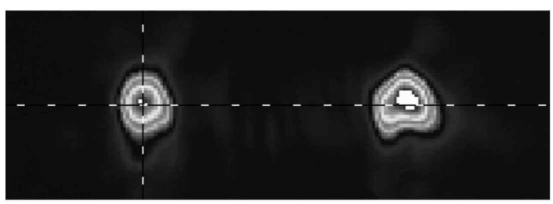

Fig. 16. Two output beams for the parabola deflector (38.6 mm long and 450 μm wide).

(a)

(b)

Fig. 17. Two output spots from the incoming B in the half-horn deflector (spot C is on the left; spot D is on the right).

output beam spots captured by camera when testing a 38.6 mm long and 450 μm wide parabola deflector. The tested half-horn deflectors have an entrance width of 450 μm and length of 40.1 mm. All the experimental results are included in Table 2. The differences between the measured and the theoretical deflection angle are due to fabrication.

B. Experiments with New Deflectors

$LiTaO_3$ single-crystal 500 μm thick z-cut wafers were also used to build EO deflectors based on the new geometries. The prism geometries follow the geometries in Fig. 8. The parabola deflectors have a 450 μm uniform width and 56.6 mm length. The half-horn deflectors have a 450 μm width at the center and 60 mm length. A 1310 nm, linearly polarized, fiber coupled laser source, polarization-maintaining collimators, and IR camera are used to test the device.

According to the design, the input collimators are strictly aligned tangent to the trajectory curve at the point of incidence and are thus positioned at fixed angles with respect to the input facet of the crystal. Suppose that the light is captured as output spot C when a 1 kV voltage is applied and that the light is captured as the output spot D when there is no external field. Two output spots, C and D, from incident beam A or B of the half-horn device are shown in Fig. 17. The deflection angles are calculated from the distance measurements of these two output spots when the light beam is launched from A or B. Table 3 gives the deflection angles of the two EO deflectors. The deflection angles are very large compared with those produced by usual rectangular devices [4]. The experimentally measured angles are the largest deflection angles ever reported for bulk EO deflectors to our knowledge. Table 3 also lists all the insertion losses of these devices when the incident light comes from input ports A or B.

The response time of $LiTaO_3$ devices is limited only by the electrical capacitive effects and by the speed of the voltage supply [12]. The rise or fall time is defined as the time it takes from 10% of the one power level to reach 90% of the other. Using this definition, the new devices demonstrated a rise time of 1.1 μs and a fall time of 100 ns. These response times can be further improved to less than 100 ns [4] by using a better high-voltage supply with a faster rise time.

Table 3. Insertion Loss, Cross Talk, and Deflection Angle

Shape, Location	Insertion Loss (dB)	Deflect. Angle (Theor./Expt.)
Half-horn (66 mm long × 550 μm wide)		
Upper, Spot 1	4.39	3.44°/3.2°
Upper, Spot 2	3.75	
Lower, Spot 1	3.57	3.44°/3.0°
Lower, Spot 2	3.28	
Parabola (66 mm long × 550 μm wide)		
Upper, Spot 1	2.87	4°/3.1°
Upper, Spot 2	2.42	
Lower, Spot 1	2.45	4°/2.9°
Lower, Spot 2	2.57	

5. Conclusions

We demonstrated two new EO deflector configurations, the half-horn and parabolic contours, and, based on them, two new deflectors are designed and fabricated. These deflectors demonstrate 3° of steering, an average insertion loss of 3 dB, and average cross talk of −30 dB. The deflection angle of the parabola device is the largest to have been reported to date to our knowledge. EO deflectors with the potential to be building blocks for nonblocking 2 × 2 optical switches are also demonstrated.

This work was supported by the Natural Sciences and Engineering Research Council (NSERC) and industrial and government partners, through the Agile All-Photonic Networks (AAPN) Research Program.

References

1. I. P. Kaminow, *An Introduction to Electrooptic Devices* (Academic, 1974), pp. 39–70.
2. E. J. Tremblay, C. Pulikkaseril, E. Shoukry, B. Bahamin, Y. Zuo, M. Mony, P. Langlois, V. Aimez, and D. V. Plant, "A 1 × 2 fast fiber-optic switch based on electro-optic beam scanning," in *Conference on Lasers and Electro-Optics* (Optical Society of America, 2004), paper CTuFF1.
3. Y. Zuo, B. Bahamin, P. Langlois, V. Aimez, and D. V. Plant, "Packaging and performance of an ultra-fast 1 × 4 optical switch," in *Conference on Lasers and Electro-Optics* (Optical Society of America, 2005), paper CTuW2.
4. Y. Zuo, B. Bahamin, E. J. Tremblay, C. Pulikkaseril, E. Shoukry, M. Mony, P. Langlois, V. Aimez, and D. V. Plant, "1 × 2 and 1 × 4 Electro-optic switches for agile all-photonic networks," IEEE Photon. Technol. Lett. **17,** 2080–2082 (2005).
5. S. Zhu, Y. Zhu, Z. Zhang, H. Shu, H. Wang, and N. Ming, "$LiTaO_3$ crystal periodically poled by applying an external pulsed field," J. Appl. Phys. **77,** 5481–5483 (1995).
6. Q. Chen, Y. Chiu, D. N. Lambeth, T. E. Schlesinger, and D. D. Stancil, "Guided-wave electro-optic beam deflector using domain reversal in LiTaO3," J. Lightwave Technol. **12,** 1401–1404 (1994).
7. J. F. Lotspeich, "Electrooptic light-beam deflection," IEEE Spectrum, February 1968, pp. 45–52.
8. Y. Chiu, R. S. Burton, D. D. Stancil, and T. E. Schlesinger, "Design and simulation of waveguide electrooptic beam deflectors," J. Lightwave Technol. **13,** 2049–2052 (1995).

9. Y. Chiu, J. Zou, D. D. Stancil, and T. E. Schlesinger, "Shape-optimized electrooptic beam scanners: analysis, design, and simulation," J. Lightwave Technol. **17,** 108–114 (1999).
10. J. C. Fang, M. J. Kawas, J. Zou, V. Gopalan, T. E. Schlesinger, and D. D. Stancil, "Shape-optimized electrooptic beam scanners: experiment," IEEE Photon. Technol. Lett. **11,** 66–68 (1999).
11. D. A. Scrymgeour, A. Sharan, V. Gopalan, K. T. Gahagan, J. L. Casson, R. Sander, J. M. Robinson, F. Muhammad, P. Chandramani, and F. Kiamilev, "Cascaded electro-optic scanning of laser light over large angles using domain microengineered ferroelectrics," Appl. Phys. Lett. **81,** 3140–3142 (2002).
12. B. E. A. Saleh and M. C. Teich, *Fundamentals of Photonics* (Wiley, 1991), pp. 696–736.
13. Ref. 12, pp. 1–39.
14. E. L. Wooten, K. M. Kissa, A. Yi-Yan, E. J. Murphy, D. A. Lafaw, P. F. Hallemeier, D. Maack, D. V. Attanasio, D. J. Fritz, G. J. McBrien, and D. E. Bossi, "A review of lithium niobate modulators for fiber-optic communications systems," IEEE J. Sel. Top. Quantum Electron. **6,** 69–82 (2000).